A target fishing study to spot possible biological targets of fusaric acid: Inhibition of protein kinase-A and insights on the underpinning mechanisms

Food and Chemical Toxicology

A target fishing study to spot possible biological targets of fusaric acid: inhibition of protein kinase-A and insights on the underpinning mechanisms

--Manuscript Draft--

Manuscript Number:	FCT-D-21-00961R3
Article Type:	Full Length Article
Keywords:	fusaric acid; target fishing; PKA; mycotoxins; mechanism of action; Fusarium sp.
Corresponding Author:	Luca Dellafiora, Ph.D. University of Parma Parma, ITALY
First Author:	Giorgia Del Favero
Order of Authors:	Giorgia Del Favero
	Georg Aichinger
	Julia Hohenbichler
	Doris Marko
	Chiara Dall'Asta
	Luca Dellafiora, Ph.D.
Abstract:	Fusaric acid is a secondary metabolite produced by various Fusarium fungi, present with relatively high incidence in Fusarium -contaminated foods. It was already described as phytotoxic and cytotoxic. However, the understanding of its molecular mechanisms is still fragmentary and further data are needed to ensure an informed assessment of the risk related to its presence in food. This work applied an integrated in silico/in vitro approach to reveal novel potential biological activity of fusaric acid and to investigate the underpinning mechanisms. An in silico reverse screening was used to identify novel biological targets for fusaric acid. Computational results indicated as target protein kinase-A, which was confirmed with biochemical cell-free assays providing evidence of its actual inhibitory potential. Cell-based experiments on intestinal cells (HCEC cells) identified the mitochondrial network and cell membranes as potentially affected organelles, possibly resulting from PKA inhibition. The integration of 3D modeling supported the plausibility of fusaric acid-dependent inhibition. From the hazard identification perspective, considering the Low Observed Adverse Effect Level described here (0.1 mM) and the possible level of contamination in food, fusaric acid might raise concern from a food safety standpoint and the gastrointestinal tract was described as a meaningful system to investigate with priority.
Response to Reviewers:	As indicated by the Co-Editor, the manuscript has been now proof-read and edited by a native speaker to improve the language, as indicated in the acknowledgement section.

A target fishing study to spot possible biological targets of fusaric acid: inhibition of protein kinase-A and insights on the underpinning mechanisms

Giorgia Del Favero[1,2]*, Georg Aichinger[1], Julia Hohenbichler[1], Doris Marko[1] Chiara Dall'Asta[3], Luca Dellafiora[3]*

[1] Department of Food Chemistry and Toxicology, Faculty of Chemistry, University of Vienna, Währingerstraße 38, 1090 Vienna, Austria

[2] Core Facility Multimodal Imaging, Faculty of Chemistry, University of Vienna, Währingerstraße 38, 1090 Vienna, Austria

[3] Department of Food and Drug, University of Parma, Area Parco delle Scienze 27/A, 43124 Parma, Italy

Corresponding authors:

* Luca Dellafiora, Department of Food and Drug, University of Parma, Area Parco delle Scienze 27/A, 43124 Parma, Italy. Phone: +39 0521 906079. Emal: luca.dellafiora@unipr.it

* Giorgia Del Favero, Department of Food Chemistry and Toxicology, Faculty of Chemistry, University of Vienna; Core Facility Multimodal Imaging, Faculty of Chemistry, University of Vienna, Währingerstraße 38, 1090 Vienna, Austria. Phone: +43-1-4277-70803. Emal: giorgia.del.favero@univie.ac.at

Abstract

Fusaric acid is a secondary metabolite produced by various *Fusarium* fungi, present with relatively high incidence in *Fusarium*-contaminated foods. It was already described as phytotoxic and cytotoxic. However, the understanding of its molecular mechanisms is still fragmentary and further data are needed to ensure an informed assessment of the risk related to its presence in food. This work applied an integrated *in silico/in vitro* approach to reveal novel potential biological activity of fusaric acid and to investigate the underpinning mechanisms. An *in silico* reverse screening was used to identify novel biological targets for fusaric acid. Computational results indicated as target protein kinase-A, which was confirmed with biochemical cell-free assays providing evidence of its actual inhibitory potential. Cell-based experiments on intestinal cells (HCEC cells) identified the mitochondrial network and cell membranes as potentially affected organelles, possibly resulting from PKA inhibition. The integration of 3D molecular modeling supported the plausibility of fusaric acid-dependent inhibition. From the hazard identification perspective, considering the Low Observed Adverse Effect Level described here (0.1 mM) and the possible level of contamination in food, fusaric acid might raise concern from a food safety standpoint and the gastrointestinal tract was described as a meaningful system to investigate with priority.

A target fishing study to spot possible biological targets of fusaric acid: inhibition of protein kinase-A and insights on the underpinning mechanisms

Giorgia Del Favero[1,2]*, Georg Aichinger[1], Julia Hohenbichler[1], Doris Marko[1] Chiara Dall'Asta[3], Luca Dellafiora[3]*

[1] Department of Food Chemistry and Toxicology, Faculty of Chemistry, University of Vienna, Währingerstraße 38, 1090 Vienna, Austria

[2] Core Facility Multimodal Imaging, Faculty of Chemistry, University of Vienna, Währingerstraße 38, 1090 Vienna, Austria

[3] Department of Food and Drug, University of Parma, Area Parco delle Scienze 27/A, 43124 Parma, Italy

Corresponding authors:

* Luca Dellafiora, Department of Food and Drug, University of Parma, Area Parco delle Scienze 27/A, 43124 Parma, Italy. Phone: +39 0521 906079. Email: luca.dellafiora@unipr.it

* Giorgia Del Favero, Department of Food Chemistry and Toxicology, Faculty of Chemistry, University of Vienna; Core Facility Multimodal Imaging, Faculty of Chemistry, University of Vienna, Währingerstraße 38, 1090 Vienna, Austria. Phone: +43-1-4277-70803. Email: giorgia.del.favero@univie.ac.at

Abstract

Fusaric acid (FA) is a secondary metabolite produced by various *Fusarium* fungi, present with relatively high incidence in *Fusarium*-contaminated foods. It was already described as phytotoxic and cytotoxic. However, the understanding of its molecular mechanisms is still fragmentary and further data are needed to ensure an informed assessment of the risk related to its presence in food. This work applied an integrated *in silico/in vitro* approach to reveal novel potential biological activities of fusaric acid and to investigate the underpinning mechanisms. An *in silico* reverse screening was used to identify novel biological targets for fusaric acid. Computational results indicated as FA-target the protein kinase-A (PKA), which was independently validated by biochemical cell-free assays. In addition, cell-based experiments on intestinal epithelial cells (HCEC-1CT) identified the mitochondrial network and cell membranes as potentially affected organelles, possibly related to PKA inhibition. The integration of 3D molecular modeling supported the plausibility of fusaric acid-dependent inhibition. From the hazard identification perspective, considering the Low Observed Adverse Effect Level described here (0.1 mM) and the plausible levels of contamination in food commodities, fusaric acid might raise concern from a food safety standpoint and potential adverse effects on the gastrointestinal tract should be further investigated with priority.

Keywords: fusaric acid, target fishing, PKA, mycotoxins, mechanism of action, *Fusarium* sp.

1. Introduction

Fusaric acid (FA; Figure 1A), also named 5-butylpiconilic acid, is a low-molecular weight secondary fungal metabolite (179.22 g/mol) which is produced by various *Fusarium* species (Munkvold, 2017). FA was reported to be phytotoxic due to its capability to impair plant growth (Loffler and Mouris, 1992; Stipanovic et al., 2011). Moreover, it extends its toxicological potential also to mammalian cells. Hence FA is cytotoxic in virtue of its *in vitro* growth inhibitory effects in cell models, and toxic *in vivo* in several animal species (Gruber-Dorninger et al., 2017).

Recent data collected in hepatic cells identified mitochondria as potential target organelles for FA with associated oxidative stress and respective repercussions on cell metabolic competence (Abdul et al., 2020a; Abdul et al., 2020b). However, the toxicological understanding of FA is still developing and FA has been included in the list of emerging mycotoxins (Gruber-Dorninger et al., 2017). Indeed, despite the few data about its occurrence / toxicity warn of a potential risk worth being analyzed with priority, FA belongs to fungal metabolites whose relevance to food safety is not fully clarified yet.

Some FA-producing species such as *F. proliferatum* and *F. oxysporum* have wide host range and, although the systematic occurrence of FA in food is rarely monitored, FA is likely to be common in several crops and food or feed products (Munkvold, 2017). Indeed, FA has shown a relatively high incidence, though a limited number of samples are typically surveyed, with the highest concentration detected in the order of µg/g (Munkvold, 2017). Based on these considerations, and considering the shortage of toxicological data, both FA occurrence and toxicity need to be better described to provide a properly informed background of knowledge to support its risk assessment.

In this framework, our study aims to identify possible novel biological targets of FA and to investigate the possible molecular mechanisms underpinning its mode of action in intestinal cells. To this purpose, an *in silico* target fishing was used: this was based on a reverse screening approach exploiting the structural information reported in the Protein Data Bank (PDB; https://www.rcsb.org) (Berman et al.,

2000), as previously described (Dellafiora et al., 2019; Dellafiora et al., 2020b). In contrast to conventional virtual screening, which identifies the ligands of a targeted protein from a compounds database, reverse screening enables the identification of potential targets of a given compound. This is obtained by screening a large number of receptors and by examining their already characterized ligands and crystal structures (Huang et al., 2018). Specific cell-free biochemical assays were then selected based on~~on the basis of~~ computational outcomes for verification purposes. Cell-based trials completed the activity-profiling *in vitro*. In this respect, a non-tumorigenic intestinal cell line (Human Colon Epithelial Cells; HCEC-1CT) was chosen as a model system being that the intestine epithelium is reasonably exposed to FA upon ingestion of contaminated food, even before eventual systemic distribution. As a final step, the mechanism of toxicity was investigated mutually integrating live cell imaging analysis and computational results from 3D modeling.

Overall, this work provides compelling evidence describing a new biological target of FA on intestinal cells and gives insights on the mechanistic basis of its activity.

2. Material and methods

2.1 Computational analysis

2.1.1 Reverse screening

A reverse screening based on a target fishing study that previously succeeded to identify unexpected targets for small molecules was used (Dellafiora et al., 2019; Dellafiora et al., 2020b), with minor modifications. In brief, the 3D structure of FA was retrieved from the PubChem database (https://pubchem.ncbi.nlm.nih.gov; PubChem CID: 3442) (Kim et al., 2019) and it was used to query the database of ligands derived from the Chemical Component Dictionary of the Protein Data Bank (PDB;

https://www.rcsb.org) (Berman et al., 2000) that included 33616 (last database access done on 18th December 2020). The structure of FA and the PDB ligands repository were downloaded in the 3D structure-data file (.sdf) format and they were further converted to the Tripos MOL2 molecular file format (.mol2) by mean of the Open Babel toolbox (O'Boyle et al., 2011). The analysis of chemical similarities was done using the LiSiCA (Ligand Similarity using Clique Algorithm) algorithm (Legnik et al., 2015). This algorithm provides a fast ligand-based virtual screening platform to search for chemical similarities between a reference compound and a database of target compounds, and it expresses similarities using the Tanimoto coefficient, a gold standard to quantify chemical analogies. LiSiCA's default parameters were used, with the exception of considering the 3D structure of ligands with the maximum allowed atom spatial distance for 3D product graph set at 2.

2.1.2 Docking study

Docking simulations were performed using the GOLD software (Genetic Optimization for Ligand Docking, version 2020) as it already showed reliability to compute protein-ligand interactions (~~e.g.~~e.g., ref. (Maldonado-Rojas and Olivero-Verbel, 2011; Rollinger et al., 2006)). The protein and ligands were processed as previously described (Dellafiora et al., 2013) with minor modifications. The protein model was derived from the crystallographic murine structure of the protein kinase A (PKA) having PDB code 4DH1 (Kovalevsky et al., 2012) that was further "humanized" introducing mutations to revert the murine protein structure to the human sequence. Of note, there were human structures of PKA, however the need to run molecular dynamic simulations in a next step of analysis made it necessary to use a humanized model (further details are reported below).

To humanize the murine structure, mutations were introduced with the "Mutate Monomers" option in the "Biopolymer" module of Sybyl, version 8.1 (www.certara.com), as previously described (Dellafiora et al., 2020a). The murine and human structures share 97.7% of sequence identity and the crystallographic

structures differ for the following residues that were mutated to obtain the humanized model: Thr32Ser, Ser34Ala, Gln39His, Asp44Glu, Ser65Thr, Ala124Pro and Thr348Ser.

ATP (Adenosine triphosphate; Figure 1C) and a PDB ligand having code 46L (Figure 1B) were also included in the docking study for a comparative purpose to FA. Their structure was derived from the structures having PDB code 4DH1 and 5N3E, respectively, and they were checked for the correctness of atoms and bonds type assignment with Sybyl, version 8.1 (www.certara.com).

The GOLD's internal scoring functions GOLDScore and PLPScore were used to score docking poses to pursue a double-function consensus scoring to enhance the prediction. In this respect, the use of multiple scoring functions, which ~~weight~~ diversely weight the contributors to the binding event, is a common practice in docking study to enhance the reliability of calculations. In particular, the agreement of the two scoring functions in terms of compounds ranking would ~~have~~ make ~~more robust~~ the prediction of PKA complexes more robust. Briefly, GoldScore has been optimized for the prediction of ligand binding positions and takes into account factors such as H-bonding energy, van der Waals energy, metal interaction and ligand torsion strain. PLPScore uses the ChemScore hydrogen bonding term and multiple linear potentials to model van der Waals and repulsive terms. Recent validation tests have shown it to be generally more effective than the other scoring functions for both pose prediction and virtual screening, according to the manufacturer declaration (https://www.ccdc.cam.ac.uk/). In each docking study, the protein was kept semi-flexible setting the polar hydrogen atoms free to rotate, while the ligands were set fully flexible.

2.1.3 Pharmacophoric analysis

The pocket was defined using GetCleft (Gaudreault et al., 2015), while the respective pharmacophoric ~~imagines~~ fingerprint were derived using the IsoMIF (Chartier and Najmanovich, 2015). Default

parameters were used. As exception, the maximum distance value between the grid and residues atoms was set at 3, and a grid resolution of 1 Å was used.

2.1.4 Molecular dynamics

Molecular dynamic simulations were performed to investigate the ligand-dependent conformational change of PKA over the time using GROMACS (version 5.1.4) (Abraham et al., 2015) with CHARMM27 all-atom force field parameters support (Best et al., 2012).

All ligands (FA, ATP and 14-22 amide; see below) have been processed and parameterized with CHARMM27 all-atom force field using the SwissParam tool (http://www.swissparam.ch) (Zoete et al., 2011). Input structures were solvated with SPC/E waters, which represents a standard pre-equilibrated 3-point solvent water model environment, in a cubic periodic boundary condition, and counter ions (Na^+ and Cl^-) were added to neutralize the system.

Prior to MD simulation, the systems were energetically minimized to avoid steric clashes and to correct improper geometries using the steepest descent algorithm with a maximum of 5,000 steps. Afterwards, all the systems underwent isothermal (300 K, coupling time 2psec) and isobaric (1 bar, coupling time 2 psec) 100 psec simulations before running 50 nsec simulations (300 K with a coupling time of 0.1 psec and 1 bar with a coupling time of 2.0 psec).

Of note, as stated above, a humanized model structure was used instead of using a human structure. This choice was necessitated ~~by the need~~ to additionally calculate ~~also~~ the dynamic of PKA in complex with the well-known inhibitor 14-22 amide, used as positive control in experimental trials (see below). Specifically, this inhibitor is a myristoylated peptide derivative having the sequence Myr-Gly-Arg-Thr-Gly-Arg-Arg-Asn-Ala-Ile-NH_2 and no structures of PKA in complex with 14-22 amide were available at the time of analysis making necessary its modeling. Many PKA structures are co-crystallized with pseudo-substrate inhibitors and ATP, but, at the time of analysis, no human structures showed inhibitors

containing the sequence Gly-Arg-Thr-Gly-Arg-Arg-Asn-Ala-Ile, which could have been used as a valid template to derive a reliable binding architecture of 14-22 amide. Conversely, the murine structure having PDB code 4DH1 is co-crystallized with ATP and the bound pseudo-substrate inhibitor included the abovementioned sequence. Therefore, the murine sequence was humanized first, as described above, and then used to derive a PKA-14-22 amide complex editing the humanized PKA-ATP-pseudo-substrate inhibitor complex with Sybyl (version 8.1; www.certara.com) to change the structure of the pseudo substrate inhibitor to that of the 14-22 amide. This structure was used as input in molecular dynamics for PKA-14-22 amide complex, while the best scored binding poses calculated by docking simulations according to the GOLDScore function were used as input for PKA-FA complex.

2.2 Experimental analysis

2.2.1 Chemicals and reagents

FA (Cat. F6513; purity ≥98%) and PKA inhibitor 14-22 amide (Cat. 476485; purity ≥95%) were acquired from SIGMA-Aldrich and dissolved according to the specification of the supplier. The PKA Kinase Enzyme System / ADP-GloTM Kinase Assay kit was purchased from Promega (Mannheim, Germany). Non-cancerous human colonic epithelial cells (HCEC-1CT) were kindly provided by Prof. J. W. Shay (UT Southwestern Medical Center, Dallas, TX, USA) (Roig et al., 2010a; Roig et al., 2010b).

2.2.2 Cell-free biochemical assay

The PKA Kinase Enzyme System / ADP-GloTM Kinase Assay kit was purchased from Promega (Mannheim, Germany) and carried out according to the manufacturer's manual. In brief, 0.5 µg/mL recombinant PKA enzyme was diluted in a reaction buffer, supplemented with 100 µM ATP and 0.5 µg/µL kemptide, and incubated in the presence of a solvent control (1% v/v DMSO), different concentrations of FA or 5 µM 14-22 amide (serving as a positive control) for 15 min. The turnover of ATP to ADP was measured by

degradation of the remaining ATP and a subsequent 30 min incubation with kinase detection reagent, leading to ADP-dependent luminescence that was measured with a BioTekTM Synergy H1 microplate reader. “No enzyme” (Incubation of reaction buffer + solvent, without PKA) and ADP controls (100 µM ADP in reaction buffer) were included to confirm full functionality of the assay kit. For data evaluation, the mean value of “no enzyme” controls ~~was~~were subtracted from respective means of the test incubation, the resulting values were related to the solvent control. Raw luminescence data was used for statistical analysis in OriginPro 2019.

2.2.3 Cell culture

HCEC-1CT cells (Roig et al., 2010a) were cultivated as previously described (Del Favero et al., 2018b) in DMEM high glucose supplemented with: 2% (v/v) Medium 199 (10X, Gibco), 2% (v/v) Hy CloneTM Cosmic Calf TM Serum, 50 µg/mL gentamicin, 20 mM 4-(2-hydroxyethyl)-1-piperazineethanesolfonic acid, insulin-transferrin-selenium-g (10 µg/mL; 5.5 µg/mL; 6.7 ng/mL), 1 µg/mL hydrocortisone and 18.7 ng/mL recombinant human epidermal growth factor. Cells were passaged every 3-4 days at 70-80% of confluency, and routinely tested for mycoplasma contamination. Cell culture media components were purchased from GIBO Invitrogen (Karlsruhe, Germany), Sigma-Aldrich (Munich, Germany) and cell culture plastic ware at Sarstedt AG & Co. (Nuembrecht, Germany) and ibidi (Gräfelfing, Germany). FA was dissolved in DMSO, 14-22 amide was solubilized in distilled water, this resulting in a final concentration of 1% (v/v) DMSO for incubation conditions.

2.2.4 Cytotoxicity testing

For cytotoxicity testing 4000 cells were seeded in 96 well plates for 48 hours. At roughly 80% of confluency cells were incubated with the respective compounds for 24 hours. After 24 hours, incubation medium was exchanged for a 1:10 dilution of CellTiter® Blue (10X, Promega) within DMEM (no phenol red) and incubated again for 50 minutes within the incubator. Subsequently fluorescence of CellTiter®

Blue medium was measured at 560nmex/590nmem utilizing a CytationTM5 Cell Imaging Multi-Mode Reader (Biotek Instruments, Inc., Winooski, VT, USA) using the Gen 5.08 software. Metabolic activity measurements were normalized to the solvent control.

2.2.5 Microscopy sample preparation

Cells were seeded on Ibitreat slides for live cell imaging. Staining was performed as previously described (Del Favero et al., 2020; Del Favero et al., 2018a) with CellMaskTM Deep Red Plasma membrane Stain (1:1000 dilution, C10046, depicted in white) and MitoTrackerTM Green FM (1:1000 dilution, M7514, depicted in blue to red). After staining, the cells were rinsed and maintained in Live Cell Imaging solution (Thermofisher). Images were acquired within 1 hour from the staining to avoid artefacts and controls were imaged at the beginning and at the end of the experimental session to ensure stability of the system. Images were acquired with a Confocal LSM Zeiss 710 equipped with ELYRA PS. 1 system using a Plan Apochromat 63X/1.2 Water objective. Images analysis results from the quantification of n≥45 ROIs (region of interest) and every experimental condition was measured in triplicate. Graphical rendering and fluorescence data (relative fluorescence units, r.f.u.) were derived with the Zeiss-ZEN software.

2.3 Statistical analysis

Data of cell-free biochemical assay are reported as mean~~s~~ ± SD of in total 6 measurements acquired in 3 independent experiments (each carried out in duplicate). Cell viability data are mean of n > 3 independent experiments ± SD. Significant differences were assessed by one-way ANOVA, followed by Fisher LSD post-hoc ~~testing~~testing, and eventually verified with Bonferroni, Scheffe, Tukey, Sidak, Bonholm, Sidakholm post-hoc tests. Data groups were considered different applying a threshold (*p*) value of 0.05. For data analysis and graphical representation, the software OriginPro 2019 was used.

2.4 Estimate of theoretical exposure

The calculation of a theoretical worst case exposure scenario (i.e., considering the highest contamination for the food category considered and a total bioavailability of FA) was based on the contamination levels of dry figs and cocoa powder reported by Di Sanzo and coworkers (Di Sanzo et al., 2018). In particular, ~~it was calculated~~ the quantity (grams) of foods bearing a total amount of FA able to determine a final concentration in ~~-~~ fasting stomach, small and large intestine near or above the LOAEL concentration value reported here (1 mM) was calulated. The volume of fasting stomach, small and large intestine used in the calculation was 47, 83 and 8 mL, respectively, according to Schiller and co-workers (Shiller et al., 2005).

3. Results and Discussion

3.1 Computational results

A reverse screening was performed first to preliminarily identify new possible biological targets of FA. In agreement with previous studies (Dellafiora et al., 2019; Dellafiora et al., 2020b), the screening was based on a target fishing study that explored the chemical space of the Protein Data Bank (PDB; https://www.rcsb.org) (Berman et al., 2000) to find low molecular weight molecules similar to FA and with already characterized biological targets. In brief, PDB includes thousands of low molecular weight molecules (more than 30000) co-crystallized with more than 170000 macromolecules (last database access on 31st December 2020). Keeping in mind that compounds sharing chemical similarities may interact with the same protein possibly resulting in a similar response in cells, mapping chemical analogies between a certain query compound and those reported in PDB may drive the identification of novel protein targets for the query under analysis, as previously described (Huang et al., 2018). To do so, FA was used as the reference molecule to screen the molecules included in the Chemical Component Dictionary of PDB (https://www.rcsb.org) (Berman et al., 2000) that counted 33616 different compounds (last database access done on 18th December 2020). The screening was performed by means

of the LiSiCA algorithm (Legnik et al., 2015) that ranked all the molecules included in the Chemical Component Dictionary according to their chemical similarities to FA. A close search was limited to those compounds having a similarity coefficient > 0.75 to focus the analysis only on the molecules theoretically most alike ~~similar~~ to FA. As reported in Table 1, five different compounds met such criterion showing the same and high similarity score of 0.78. This facilitated the subsequent identification of five different proteins potentially worthy of further analysis. T ~~Notably, t~~he fact that all ~~those~~ five compounds recorded the same score pointed to their overall chemical equivalence according to the LiSiCA algorithm. Therefore, the output underwent a further expert visual inspection to ascertain the actual similarity of chemicals to FA as well as to examine~~check~~ the possible relevance of the respective protein(s) they are bound to. In this respect, keeping in mind that the functional inference of FA should have been made ideally on human cells, the analysis was focused on proteins from the animal kingdom first, considering those from other kingdoms only in ~~the~~ case the animal proteins are not identified at ~~a~~ first instance. This criterion complied with the principle that the closer the evolutionary relationship between proteins (and the organisms they belong to), the more likely the functional conservation of bioactive compounds, as previously demonstrated (e.g. ref. (Drakakaki et al., 2011)).

As shown in Table 1, the reverse screening identified the protein kinase A (PKA) from *Cricetulus griseus* (Chinese hamster) in the bound state with the ligand having PDB code 46L (6-(dimethylamino)pyridine-3-carboxylic acid), which had marked chemical analogies with FA, as shown in Figure 1. In particular, 46L was the unique ligand among those identified by the reverse screening that showed a pyridine core linked to a carboxylic acid. On this basis, PKA was considered a possible binding partner of FA and the analysis was~~it was~~ carried forth ~~the analysis~~ to determine~~check~~ the actual capability of FA to interact with PKA, while the other non-animal proteins were not analyzed further.

The capability of FA to interact with PKA was analyzed through docking studies and pharmacophoric analysis to investigate~~check~~ the capability of FA to dock the PKA pocket, followed by molecular dynamic

simulations to verifycheck the capability of FA to persist therein. In agreement with the protonation state suggested for 46L in the crystallographic protein-ligand complex (Oebbeke et al., 2021), FA was computed with the carboxylic moiety in the protonated state. In this respect, although the pKa of benzoic acid-related compounds would suggest the deprotonated state as preferential in a physiological condition, evidence previously reported described the possibility of carboxylic acids to circumstantially hold a fully localized proton (Lin et al., 2017), as in this case. Concerning the binding site of PKA that was analyzed in this study, 46L was described to bind the ATP binding site (Oebbeke et al., 2021). Therefore, FA was docked within the ATP binding site of a PKA model (further details about the model construction are reported in Materials and Methods section). ATP and 46L were also included as well in the docking study for comparison and validation purposes. As shown in Figure 2, the docking pose of FA was able to well retrace the binding mode of 46L adequately, partially mimicking the pattern of interaction described for ATP by crystallographic studies, engaging with hydrogen bonds the amidic nitrogen and carbonyl oxygen of Val123 and Glu121, respectively. In addition, the docking of ATP and 46L provided a binding architecture resembling those respectively reported in crystallographic studies (e.g.e.g., ref. (Kovalevsky et al., 2012; Oebbeke et al., 2021)), supporting the geometrical reliability of the model used. In this respect, both the scoring functions used to score the binding pose of ligands recorded scores much higher for ATP compared to FA and 46L. In particular, ATP (was) scored 109 and 122 units, while FA (was) scored 45 and 42 units, and 46L (was) scored 43 and 39, according to PLPScore and GOLDscore scoring functions respectively. The agreement of the two scoring functions enhanced the prediction soundness (for further information see section 2.1.2). Of note, both scoring functions provide scores theoretically proportional to the capability of ligands to fit the corresponding protein pocket (the higher the score, the better the fitting within pockets) (Dellafiora et al., 2019). Therefore, they may circumstantially allow a (semi)quantitative comparison of ligands. On this basis, although a proper validation of the method used was not done due to a shortage of data for deriving a suitable validation

set of compounds, it was hypothesized, as expected, that ATP is a better ligand for the pocket compared to FA or 46L.

In addition to that, the molecule having PDB code 46L arose from a fragment-based screening campaign (Oebbeke et al., 2021) and ~~,~~ although the binding affinity was not assessed, fragment-based screening typically provides lead compounds with weak pharmacological/binding properties that serve as a scaffold to derive optimized and pharmacologically relevant derivatives (Li, 2020). Therefore, the analogies between FA and 46L might suggest a relatively low capability to bind the PKA pocket. However, the pharmacophoric analysis (Figure 2) suggested a theoretically higher capability of FA to satisfy the pocket compared to 46L, due to the lipophilic *para* aliphatic portion that well-matched with the hydrophobic region of the pocket it was found arranged into. Conversely, 46L arranged the tertiary amine therein, which is supposed to retain a higher degree of polarity compared to the aliphatic tail of FA, possibly~~likely~~ causing a certain degree of hydrophilic/hydrophobic interference. This observed theoretical higher capability of FA to dock the pocket was in agreement with the docking scores of 46L, which were both lower than those of FA (as reported above).

Afterwards, the dynamic of interaction of FA with PKA was analyzed through molecular dynamics and compared to that of PKA in complex with the 14-22 amide, a well-known PKA inhibitor used as a positive control in experimental trials (see below). The analysis aimed at testing~~checking~~ the capability of FA to persist at the PKA binding site over time, as well as confirming~~at checking~~ differential FA-dependent protein reorganization compared to the PKA in complex with 14-22 amide. The analysis measured ligands and protein root-mean-square deviation (RMSD) to monitor the geometrical stability of ligands and the evolution of protein conformation over time. The root-mean-square fluctuation (RMSF) and the ligands trajectories were also analyzed to investigate~~check~~ ligand-dependent local effects on protein organization and the actual capability of ligands to persist at the PKA pocket. As shown in Figure 3, the overall organization of PKA was found stable in complex either with FA or 14-22 amide, although the

complex with FA showed RMSD values higher than those of PKA in complex with 14-22 amide in most of the timeframe considered. This result indicated that FA induced an early and more significant change of the starting PKA conformation compared 14-22 amide as a possible result of a FA-induced conformational fit. The RMSD analysis of ligands revealed that both were geometrically stable during the whole simulation. However, 14-22 amide showed higher values compared to FA as a consequence of an early reorganization of the myristic acid-terminal moiety, while the rest of the molecules were~~was~~ kept stably organized during the whole simulation. The analysis of ligand trajectories confirmed their capability to persist at the designated binding site during the whole simulation and confirmed the local reorganization of the myristic acid-terminal moiety of 14-22 amide. Particularly, FA and 14-22 amide had two distinct binding sites as the former was found to interact within the ATP binding cleft, while the latter interacted at the substrate binding site. A close inspection of local motions through the RMSF analysis revealed some differences between the two PKA complexes. Indeed, six regions were found to have a differential mobility and four of them in the PKA-FA complex were found interested by a less stable organization compared to PKA-14-22 amide complex. As shown in Figure 3, the most extended zones with an enhanced motion were found to form the area surrounding the region contacting substrates (residues 152-171 and 179-209), part of the region close to the ATP binding site, and a solvent-exposed surface aside (residues 335-342). It is reasonable to hypothesize that such FA-induced reorganization of PKA structure may influence the capability of PKA to contact its biological targets. In this respect, although the mechanistic understanding of PKA action still remains incomplete, it has been reported that PKA has many biological targets mediating its biological role, which goes beyond the simple kinase activity, including substrate, pseudo-substrate and non-substrate proteins (Soberg and Skalhegg, 2018). In particular, the possibility to interact with non-substrate partners is important to anchor the catalytic subunit of PKA at a sub-cellular level, although the underpinning mechanisms of PKA anchoring and the consequences of its disruption are not fully understood yet (Soberg and

Skalhegg, 2018). On this basis, FA might have a multifaceted role on PKA in cells including either the reduction of its catalytic activity by competing with ATP, or by changing its capability to contact the plethora of its protein partners.

3.2 Experimental results

Building on the computational results, validation experiments were performed to explore the capability of FA to inhibit PKA in a cell-free ~~condition .~~condition. As shown in Figure 4A, the incubation of recombinant PKA with FA led to a concentration-dependent inhibition of its enzymatic activity, which was statistically significant at the highest applied dose (1 mM FA, 70.2% ± 5.1% activity). The 14-22 amide, a well-known PKA inhibitor (Harris et al., 1997), was used as a positive control, while ADP (adenosine di-phosphate) was used as a negative control, in agreement with the assay instructions. Although FA showed a relatively mild inhibitory activity in cell-free conditions, the results supported the outcome of the computational prediction.

Furthermore, *in silico* analysis pointed toward the potential of FA to change the organization of PKA regions other than those involved in the interaction with substrates. This obviously reflects in a manifold action at cellular level. In this respect, keeping in mind the complexity of PKA functionality (Morrison, 2021) and based on recent data reporting mitochondria as potential target organelles for FA (Abdul et al., 2020a; Abdul et al., 2020b), proof of principle experiments were additionally performed in an intestinal epithelial cells model. This included the impact of the food-borne contaminant on cell viability, as well as mechanistic toxicity assessment through live cell imaging taking the effect on the mitochondria as reference. Consistent with the cell-free assay, cytotoxicity experiments showed a significant decrease of cell viability after incubation with 1 mM FA (Figure 4B). Analogue to this~~In~~

~~parallel,~~ the PKA inhibitor (PKAi) 14-22 amide did not hamper cell viability at the concentration of 5 µM, making its use possible for further mechanistic studies.

~~On the basis of~~Based on cytotoxicity data and enzymatic assay, concentrations 0.1 and 1 mM were selected for further live cell imaging experiments representing the NOAEL (No Observed Adverse Effect Level) and LOAEL (Lowest Observed Adverse Effect Level) for the system. As for our hypothesis, FA affected the integrity of the mitochondria in a treatment-dependent manner. Upon incubation with 0.1 mM FA the mitochondrial network was characterized by more elongated organelles and a significant increase of the mitochondrial-associated signal. This readout is compatible with the onset of a stress response possibly mirroring the beginning of metabolic adaption and/or oxidative stress imbalance. At the concentration of 1 mM the mitochondrial network appeared completely and severely fragmented (Figure 5A). Furthermore ~~In parallel,~~ concentration-dependent degradation of the cell membrane could be observed (Figure 5A and D).

Interestingly, the performance of the experiment in presence of the PKA inhibitor 14-22 amide resulted in a partial reduction of the abovementioned effects. This included a recovery in the mitochondrial network as well as an amelioration of the membrane appearance and associated signal (Figure 5B-D). Image analysis supported the morphological description. In agreement with our line of interpretation, the presence of PKA inhibitor 14-22 amide re-established the concentration dependency in the FA-mediated mitochondrial response, possibly preventing/slowing excessive mitochondrial damage (Figure 5C). Similarly, cell membrane signal did not drop in intensity when FA was co-incubated with 14-22 amide, and the signal profile retraced in the dose-response provided a pattern similar to the one of the mitochondria (Figure 5C-D). Overall, these data suggest the existence of ~~a~~ crosstalk between FA and PKA inhibitor 14-22 amide and hint a functional PKA to be central in sustaining the effects of FA on intestinal cells. Consistent with~~Supportive of~~ this line of interpretation, the PKA inhibitor 14-22 amide (5 µM) alone did not alter the readouts of control cells and proved its highest modulatory potential when co-

incubated with 1 mM FA. Taken together, the results of *in vitro* trials were in line with those observed *in silico* providing a plausible mechanistic rationale to the outcomes of cell trials. FA was predicted to alter the geometrical organization of specific regions of PKA compared to 14-22 amide with possible effects on the capability of PKA to contact protein partners. In this respect, the binding of 14-22 amide at the substrate binding site prevented the interaction of FA within the inner part of ATP binding site, as, in other words 14-22 amide occluded the entrance path of FA (Figure 6), possibly preventing the FA-induced reorganization of PKA. Therefore, the capability of 14-22 amide to modulate the activity of FA on mitochondria and cell membranes could be explained, at least in part, by the capacity of the inhibitor to avoid a FA-induced PKA reorganization. This emerged as a possible relevant mechanism among those underpinning the effects of FA on cells. Notably, the lowest concentration found effective in cells (0.1 mM) was found inactive in cell-free trials. This apparent discrepancy can be due to the diverse chemical environment of the two test systems, the multifaceted functionality of PKA (Klussmann, 2007; Robinson-White and Stratakis, 2002), as well as the relative interaction of ATP and FA described *in silico*. Specifically, as reported above, FA was described as a PKA binder endowed with~~of~~ a limited inhibitory activity in cell-free conditions. This is related to its computed inferior capability to interact with the ATP binding pocket when compared to the endogenous ligand ATP. Therefore, in over-simplified cell-free circumstances, where the functionality of PKA is limited to the transformation of a reference non-physiological substrate with a full disposability of ATP, this property might have determined a limited capability to inhibit the reporter system. Conversely, in cells, PKA functionality and its surrounding chemical environment are inherently more complex compared to the cell-free assays and , ~~,~~in this condition~~,~~ the ~~PKA~~ geometrical stability of PKA is likely to play a major role, being fundamental to recognize protein partners. This might have contributed to determine the increased sensitivity of cell-based assay to FA in comparison to cell-free experiments. The higher activity observed in cells could be also due to the plausibly diverse chemical context in which~~where~~ the local disposability of ATP for PKA

might be lower compared to the cell-free assay reducing its preventing effects on FA binding. Nonetheless, the involvement of other PKA-independent mechanisms cannot be excluded.

Concerning the relevance of the tested concentrations to the abundance of FA in contaminated food, it is important to note that data on the occurrence of FA in food are still sporadic and the exposure of human population to this mycotoxin is substantially overlooked. However, FA can be ubiquitously produced by several *Fusarium* species (Abdul et al., 2020b) and in certain food commodities it can have a high incidence with the highest concentration reported in the order of µg/g (e.g. (Di Sanzo et al., 2018; Li et al., 2013; Munkvold, 2017)). As an example, Di Sanzo and co-workers reported ~~a~~ contamination levels up to 11.283 µg/g in dried figs and 41.779 µg/g in cocoa powder (Di Sanzo et al., 2018). Consequently~~Of note~~, assuming the full release of FA from food matrix during digestion, 132, 75, and 13 grams of the highest-contaminated figs or 35, 20, and 3 grams of the highest-contaminated cocoa powders, contain the amount of FA theoretically able to determine a concentration above the LOAEL reported here (0.1 mM) in fasting stomach, small intestine and large intestine, respectively (Table 2). The actual release of FA from food matrix and its resistance during digestion need to be studied in more detail. However, dried figs and cocoa powder~~r are considered~~ with an average serving size of 50 and 5 grams respectively, implicate ~~meaning~~ that the consumption of highly contaminated servings might determine an overall exposure to FA ~~-~~able to reach or exceed the active concentration found in this study along the GI tract ~~the concentration found active in this study~~. From a food safety perspective, the active concentration depicted in this work, is of potential relevance. ~~This makes the concentration tested active in this work of potential relevance from a food safety perspective.~~ Along this line, research into bioavailability and bioaccessibility of FA should be deepened, along with determining~~checking systematically~~ its occurrence in food and the exposure of human population systematically, to support a proper risk assessment.

4. Conclusion

FA raises safety concerns because of its ubiquitous production by several *Fusarium* species; the latter commonly contaminate agriculturally important crops and are responsible for substantial FA levels (in the order of mg/Kg), as already reported in certain food commodities (Abdul et al., 2020b; Di Sanzo et al., 2018). Nonetheless, FA is a largely understudied mycotoxin and its possible relevance to the food safety area is still not well understood. Therefore, the elucidation of FA toxicity and the molecular mechanisms beneath are essential to define an informed background of knowledge to foster its risk assessment. Within the framework of describing mechanistic aspects of FA activity, the present work elucidates for the first time FA as an inhibitor of the PKA with respective effects on the mitochondria network and membrane integrity of intestinal cells. Specifically, the integrated use of *in vitro* assays, live-cell imaging and 3D molecular modeling proposed the inhibition of PKA and its subsequent FA-induced geometrical changes among the likely underpinning molecular mechanisms. Of note, although the internal exposure caused by the ingestion of contaminated food needs to be assessed further, the consumption of certain highly contaminated foods (~~e.g.~~e.g., dry figs and cocoa powder) might determine FA concentrations in the GI tract in the order of the LOAEL described here. This evidence makes the effects of FA on PKA and/or on mitochondrial functionality at the GI level of potential relevance from a real-world perspective and worth of further dedicated studies. In addition, future studies may also address the evaluation of *in vivo* or *ex vivo* effects using mouse models as they already proved to be a reliable system to study the manifold consequences of PKA inhibition (~~e.g.~~e.g., (Briassoulis et al., 2016; Morgan et al., 2008)). Keeping in mind that the toxicological understanding of FA action in animals is extremely scarce, data from *in vivo* or *ex vivo* would bring precious information to investigate the potential capability of FA to originate pathological condition of physiological deregulation in living organisms.

Acknowledgment

This research benefits from the HPC (high performance computing) facility of the University of Parma, Italy. Imaging workflows were supported by the Core Facility Multimodal Imaging of the Faculty of Chemistry (University of Vienna) member of VLSI – Vienna Life Science Instruments. The authors are grateful to Janice Arline Bergen for her precious support in formal editing and proof reading the manuscript.

References

Abdul, N.S., Nagiah, S., Anand, K., Chuturgoon, A.A., 2020a. Molecular docking and mechanisms of fusaric acid induced mitochondrial sirtuin aberrations in glycolytically and oxidatively poised human hepatocellular carcinoma (HepG2) cells. Toxicon 173, 48-56.

Abdul, N.S., Nagiah, S., Chuturgoon, A.A., 2020b. The neglected foodborne mycotoxin Fusaric acid induces bioenergetic adaptations by switching energy metabolism from mitochondrial processes to glycolysis in a human liver (HepG2) cell line. Toxicology Letters 318, 74-85.

Abraham, M.J., Murtola, T., Schulz, R., Páll, S., Smith, J.C., Hess, B., Lindahl, E., 2015. GROMACS: High performance molecular simulations through multi-level parallelism from laptops to supercomputers SoftwareX 1-2, 19-25.

Berman, H.M., Westbrook, J., Feng, Z., Gilliland, G., Bhat, T.N., Weissig, H., Shindyalov, I.N., Bourne, P.E., 2000. The Protein Data Bank. Nucleic Acid Res. 28, 235-242.

Best, R.B., Zhu, X., Shim, J., Lopes, P.E., Mittal, J., Feig, M., Mackerell, A.D.J., 2012. Optimization of the additive CHARMM all-atom protein force field targeting improved sampling of the backbone ϕ, ψ and side-chain χ(1) and χ(2) dihedral angles. J. Chem. Theory Comput. 8, 3257-3273.

Briassoulis, G., Keil, M.F., Naved, B., Liu, S., Starost, M.F., Nesterova, M., Gokarn, N., Batistatos, A., Wu, T.J., Stratakis, C.A., 2016. Studies of mice with cyclic AMP-dependent protein kinase (PKA) defects reveal the critical role of PKA's catalytic subunits in anxiety. Behavioural Brain Research 307, 1-10.

Chartier, M., Najmanovich, R., 2015. Detection of Binding Site Molecular Interaction Field Similarities. J. Chem. Inf. Model. 55, 1600-1615.

Del Favero, G., Hohenbichler, J., Mayer, R.M., Rychlik, M., Marko, D., 2020. Mycotoxin Altertoxin II Induces Lipid Peroxidation Connecting Mitochondrial Stress Response to NF-κB Inhibition in THP-1 Macrophages. Chemical Research in Toxicology 33, 492-504.

Del Favero, G., Woelflingseder, L., Janker, L., Neuditschko, B., Seriani, S., Gallina, P., Sbaizero, O., Gerner, C., Marko, D., 2018a. Deoxynivalenol induces structural alterations in epidermoid carcinoma cells A431 and impairs the response to biomechanical stimulation. Sci. Rep. 8, 11351.

Del Favero, G., Zaharescu, R., Marko, D., 2018b. Functional impairment triggered by altertoxin II (ATXII) in intestinal cells in vitro: cross-talk between cytotoxicity and mechanotransduction. Archives of Toxicology 92, 3535-3547.

Dellafiora, L., Aichinger, G., Geib, E., Sánchez-Barrionuevo, L., Brock, M., Cánovas, D., Dall'Asta, C., Marko, D., 2019. Hybrid in silico/in vitro target fishing to assign function to "orphan" compounds of food origin–The case of the fungal metabolite atromentin. Food Chem. 270, 61-69.

Dellafiora, L., Filipello, V., Dall'Asta, C., Finazzi, G., Galaverna, G., Losio, M.N., 2020a. A Structural Study on the Listeria Monocytogenes Internalin A-Human E-cadherin Interaction: A Molecular Tool to Investigate the Effects of Missense Mutations. Toxins 12.

Dellafiora, L., Mena, P., Cozzini, P., Brighenti, F., Del Rio, D., 2013. Modelling the possible bioactivity of ellagitannin-derived metabolites. In silico tools to evaluate their potential xenoestrogenic behavior. Food & Function 4, 1442-1451.

Dellafiora, L., Milioli, M., Falco, A., Interlandi, M., Mohamed, A., Frotscher, M., Riccardi, B., Puccini, P., Rio, D.D., Galaverna, G., Dall'Asta, C., 2020b. A Hybrid In Silico/In Vitro Target Fishing Study to Mine Novel Targets of Urolithin A and B: A Step Towards a Better Comprehension of Their Estrogenicity. Mol. Nutr. Food Res. 64.

Di Sanzo, R., Carabetta, S., Campone, L., Bonavita, S., Iaria, D., Fuda, S., Rastrelli, L., Russo, M., 2018. Assessment of mycotoxins co-occurrence in Italian dried figs and in dried figs-based products. Journal of Food Safety 38.

Drakakaki, G., Robert, S., Szatmari, A.M., Brown, M.Q., Nagawa, S., Van Damme, D., Leonard, M., Yang, Z.B., Girke, T., Schmid, S.L., Russinova, E., Friml, J., Raikhel, N.V., Hicks, G.R., 2011. Clusters of bioactive compounds target dynamic endomembrane networks in vivo. Proc. Natl. Acad. Sci. U. S. A. 108, 17850-17855.

Gaudreault, F., Morency, L.P., Najmanovich, R.J., 2015. NRGsuite: a PyMOL plugin to perform docking simulations in real time using FlexAID. Bioinformatics 31, 3856-3858.

Gruber-Dorninger, C., Novak, B., Nagl, V., Berthiller, F., 2017. Emerging Mycotoxins: Beyond Traditionally Determined Food Contaminants. J. Agr. Food Chem. 65, 7052-7070.

512 Harris, T.E., Persaud, S.J., Jones, P.M., 1997. Pseudosubstrate inhibition of cyclic AMP-dependent protein
513 kinase in intact pancreatic islets: Effects on cyclic AMP-dependent and glucose-dependent insulin
514 secretion. Biochemical and Biophysical Research Communications 232, 648-651.

515 Huang, H.B., Zhang, G.G., Zhou, Y.Q., Lin, C.R., Chen, S.L., Lin, Y.T., Mai, S.K., Huang, Z.N., 2018. Reverse
516 Screening Methods to Search for the Protein Targets of Chemopreventive Compounds. Front. Chem. 6.

517 Kim, S., Chen, J., Cheng, T.J., Gindulyte, A., He, J., He, S.Q., Li, Q.L., Shoemaker, B.A., Thiessen, P.A., Yu,
518 B., Zaslavsky, L., Zhang, J., Bolton, E.E., 2019. PubChem 2019 update: improved access to chemical data.
519 Nucleic Acid Res. 47, D1102-D1109.

520 Klussmann, E., 2007. Protein Kinase A, in: S.J. Enna, D.B. Bylund (Eds.), xPharm: The Comprehensive
521 Pharmacology Reference. Elsevier, pp. 1-9.

522 Kovalevsky, A.Y., Johnson, H., Hanson, B.L., Waltman, M.J., Fisher, S.Z., Taylor, S., Langan, P., 2012. Low-
523 and room-temperature X-ray structures of protein kinase A ternary complexes shed new light on its
524 activity. Acta Crystallographica Section D-Biological Crystallography 68, 854-860.

525 Legnik, S., Stular, T., Brus, B., Knez, D., Gobec, S., Janezic, D., Konc, J., 2015. LiSiCA: A Software for
526 Ligand-Based Virtual Screening and Its Application for the Discovery of Butyrylcholinesterase Inhibitors.
527 J. Chem. Inf. Model. 55, 1521-1528.

528 Li, C.Y., Zuo, C.W., Deng, G.M., Kuang, R.B., Yang, Q.S., Hu, C.H., Sheng, O., Zhang, S., Ma, L.J., Wei, Y.R.,
529 Yang, J., Liu, S.W., Biswas, M.K., Viljoen, A., Yi, G.J., 2013. Contamination of Bananas with Beauvericin
530 and Fusaric Acid Produced by Fusarium oxysporum f. sp cubense. Plos One 8.

531 Li, Q.X., 2020. Application of Fragment-Based Drug Discovery to Versatile Targets. Frontiers in Molecular
532 Biosciences 7.

Lin, J.S., Pozharski, E., Wilson, M.A., 2017. Short Carboxylic Acid-Carboxylate Hydrogen Bonds Can Have Fully Localized Protons. Biochemistry 56, 391-402.

Loffler, H.J.M., Mouris, J.R., 1992. FUSARIC ACID - PHYTOTOXICITY AND INVITRO PRODUCTION BY FUSARIUM OXYSPORUM F-SP LILII, THE CAUSAL AGENT OF BASAL ROT IN LILIES. Netherlands Journal of Plant Pathology 98, 107-115.

Maldonado-Rojas, W., Olivero-Verbel, J., 2011. Potential interaction of natural dietary bioactive compounds with COX-2. J. Mol. Graph. Model. 30, 157-166.

Morgan, D.J., Weisenhaus, M., Shum, S., Su, T., Zheng, R.M., Zhang, C., Shokat, K.M., Hille, B., Babcock, D.F., McKnight, G.S., 2008. Tissue-specific PKA inhibition using a chemical genetic approach and its application to studies on sperm capacitation. Proc. Natl. Acad. Sci. U. S. A. 105, 20740-20745.

Morrison, H., 2021. Chapter 29 - Protein kinase A, in: H. Morrison (Ed.), Enzyme Active Sites and their Reaction Mechanisms. Academic Press, pp. 173-178.

Munkvold, G.P., 2017. Fusarium Species and Their Associated Mycotoxins. Methods in Molecular Biology 1542, 51-106.

O'Boyle, N.M., Banck, M., James, C.A., Morley, C., Vandermeersch, T., Hutchison, G.R., 2011. Open Babel: An open chemical toolbox. Journal of Cheminformatics 3.

Oebbeke, M., Siefker, C., Wagner, B., Heine, A., Klebe, G., 2021. Fragment Binding to Kinase Hinge: If Charge Distribution and Local pK(a) Shifts Mislead Popular Bioisosterism Concepts. Angewandte Chemie-International Edition 60, 252-258.

552 Robinson-White, A., Stratakis, C.A., 2002. Protein kinase A signaling - "Cross-talk" with other pathways in
553 endocrine cells, in: C.A. Stratakis, Y.S. ChoChung (Eds.), Protein Kinase a and Human Disease, pp. 256-
554 270.

555 Roig, A.I., Eskiocak, U., Hight, S.K., Kim, S.B., Delgado, O., Souza, R.F., Spechler, S.J., Wright, W.E., Shay,
556 J.W., 2010a. Immortalized Epithelial Cells Derived From Human Colon Biopsies Express Stem Cell
557 Markers and Differentiate In Vitro. Gastroenterology 138, 1012-U1272.

558 Roig, A.I., Eskiocak, U., Hight, S.K., Kim, S.B., Delgado, O., Souza, R.F., Spechler, S.J., Wright, W.E., Shay,
559 J.W., 2010b. Immortalized epithelial cells derived from human colon biopsies express stem cell markers
560 and differentiate in vitro. Gastroenterology 138, 1012-1021.e1015.

561 Rollinger, J.M., Schuster, D., Baier, E., Ellmerer, E.P., Langer, T., Stuppner, H., 2006. Taspine: bioactivity-
562 guided isolation and molecular ligand-target insight of a potent acetylcholinesterase inhibitor from
563 Magnolia x soulangiana. J. Nat Prod. 69, 1341-1346.

564 Schiller, C., Frohlich, C.P., Giessmann, T., Siegmund, W., Monnikes, H., Hosten, N., Weitschies, W., 2005.
565 Intestinal fluid volumes and transit of dosage forms as assessed by magnetic resonance imaging.
566 Alimentary Pharmacology & Therapeutics 22, 971-979.

567 Soberg, K., Skalhegg, B.S., 2018. The Molecular Basis for Specificity at the Level of the Protein Kinase a
568 Catalytic Subunit. Frontiers in Endocrinology 9.

569 Stipanovic, R.D., Puckhaber, L.S., Liu, J., Bell, A.A., 2011. Phytotoxicity of fusaric acid and analogs to
570 cotton. Toxicon 57, 176-178.

571 Zoete, V., Cuendet, M.A., Grosdidier, A., Michielin, O., 2011. SwissParam: A Fast Force Field Generation
572 Tool for Small Organic Molecules. J. Comput. Chem. 32, 2359-2368.

573

574 **Tables**

Table 1. Results of reverse screening

Similarity Score*	Ligand ID	Protein bound	Organism
1.00	CQV	Purine Nucleoside Phosphorylase Isoform 2	*Schistosoma mansoni*
0.79	8ZU	CYP199A4	*Rhodopseudomonas palustris HaA2*
0.79	8QM	CYP199A4	*R. palustris*
0.79	4IA	CYP199A4	*R. palustris HaA2*
		Mutant CYP199A4 (T252A)	*R. palustris HaA2*
		tRNA-Guanine Transglycosylase	*Zymomonas mobilis*
0.79	46L	Protein Kinase A (PKA)	*Cricetulus griseus*
		Endothiapepsin	*Cryphonectria parasitica*

* Similarity score has been computed using the LiSiCA algorithm (Legnik et al., 2015) and it is based on the Tanimoto's coefficient that ranges from 0 (structurally unrelated compounds) to 1 (for identical compounds).

575

576

Table 2. Calculated quantities (serving size) of dry figs and cocoa powder which would reach a concentration of 0.1 mM FA (LOAEL in this study) in fasting stomach, small intestine, or large intestine assuming commodities contamination levels reported by Di Sanzo et al., 2018.

	Stomach	Small intestine	Large intestine
Dry figs	75 gr	132 gr	13 gr
Cocoa powder	20 gr	35 gr	3 gr

Note: the median volume of fasting stomach, small intestine and large intestine reported by Schiller and coworkers (Schiller et al., 2005) was used as reference (i.e. 47, 83 and 8 mL, respectively).

577

578 **Figures**

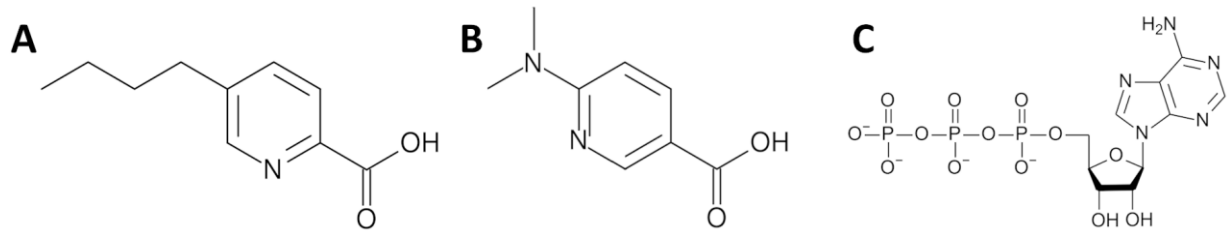

579

580 **Figure 1.** Chemical structure of the main compounds under analysis. **A.** Fusaric acid. **B.** 46L (6-
581 (dimethylamino)pyridine-3-carboxylic acid). **C.** ATP (Adenosine triphosphate)

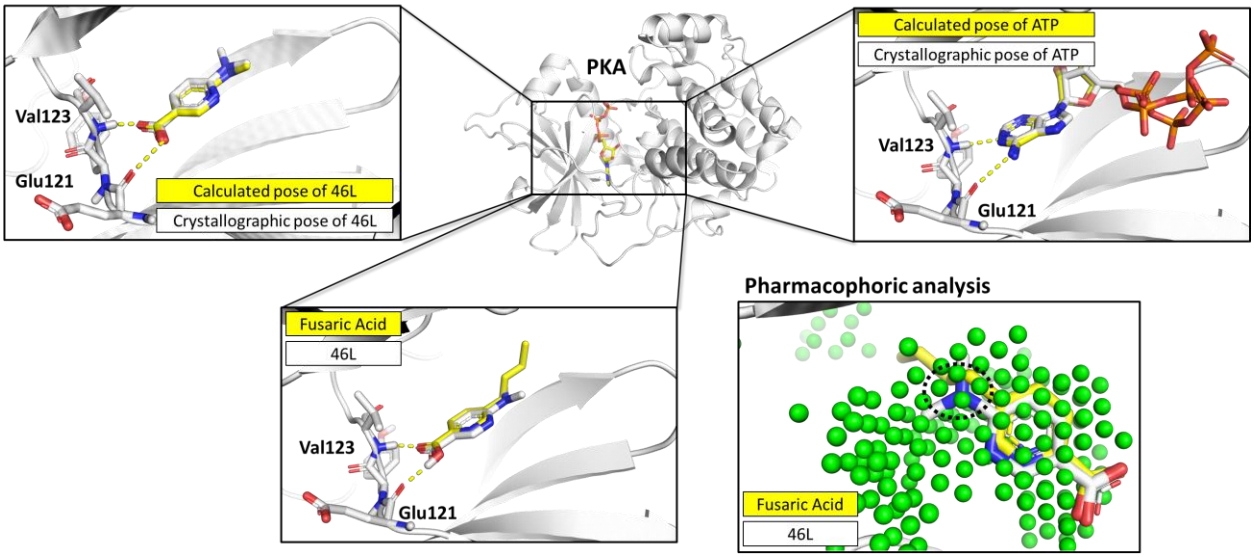

582

583 **Figure 2.** Docking results and pharmacophoric analysis. The PKA is represented in white cartoon, while
584 close-ups represent the ATP binding site with the calculated pose of FA or 46L (colored in yellow) in
585 comparison to the crystallographic pose of 46L (colored in white; as reported in the PDB structure
586 having code 5N3E), or the calculated pose of ATP (colored in yellow) in comparison to its
587 crystallographic structure (colored in white; as reported in the PDB structure having code 4DH1). Ligands
588 and residues involved in polar contacts are represented in sticks, while the yellow dashed lines indicate
589 the hydrogen bonds. In the pharmacophoric analysis, green spheres indicate regions sterically and
590 energetically able to receive hydrophobic groups. The dashed black circle indicates the improper
591 arrangement of the 46L's amino group within the hydrophobic space of the pocket.

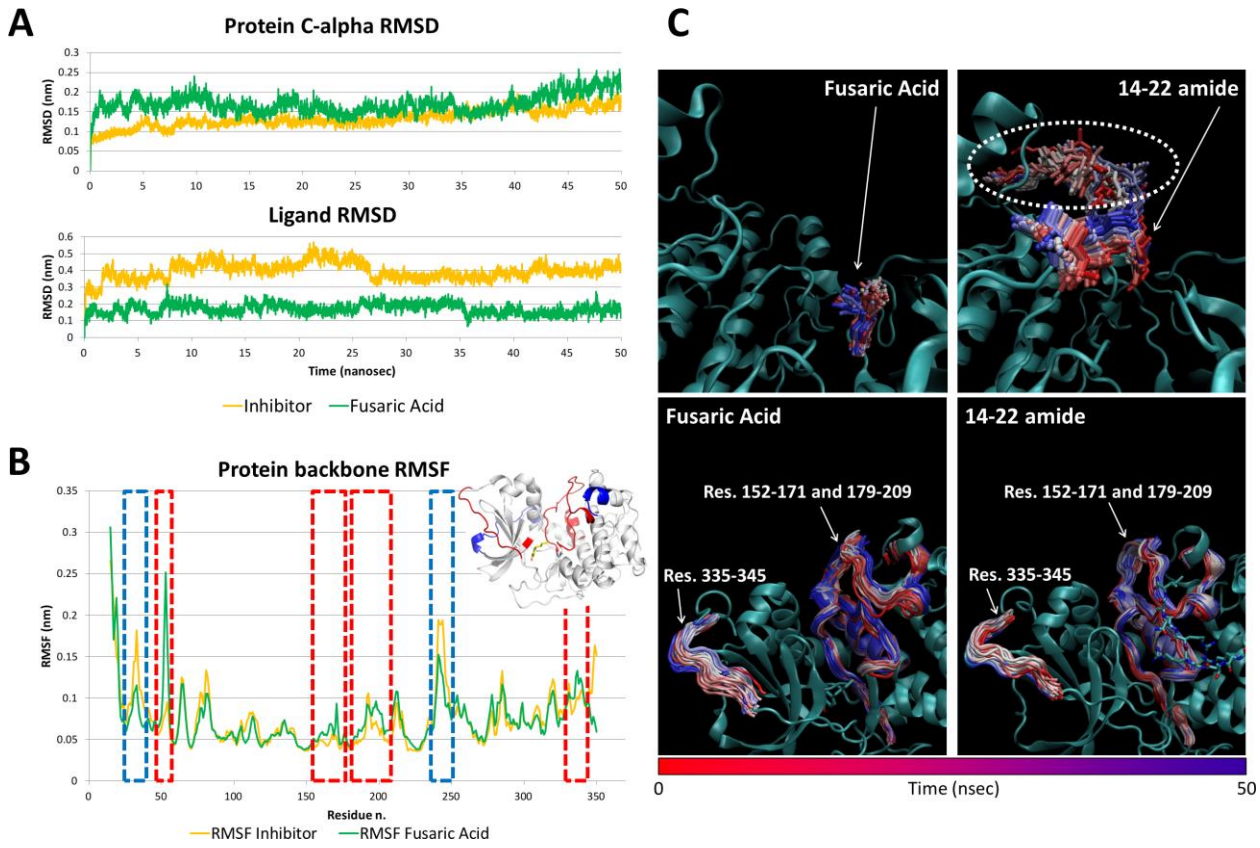

592

593 **Figure 3.** Molecular dynamics results. **A.** RMSD of protein and ligands. **B.** RMSF analysis. Blue and red
594 dashed boxes indicate the region of the PKA-FA complex that showed a higher and lower mobility,
595 respectively, compared to the PKA-14-22 amide complex. These regions are colored accordingly in the
596 cartoon representation of PKA (upper-left corner). **C.** Time-step representation of ligand and protein
597 trajectories of PKA in complex with FA or 14-22 amide. The dashed with ring indicates the mirystic acid-
598 terminal moiety of 14-22 amide. The from-red-to-blue color switch indicates the stepwise changes of
599 coordinates along the MD simulation.

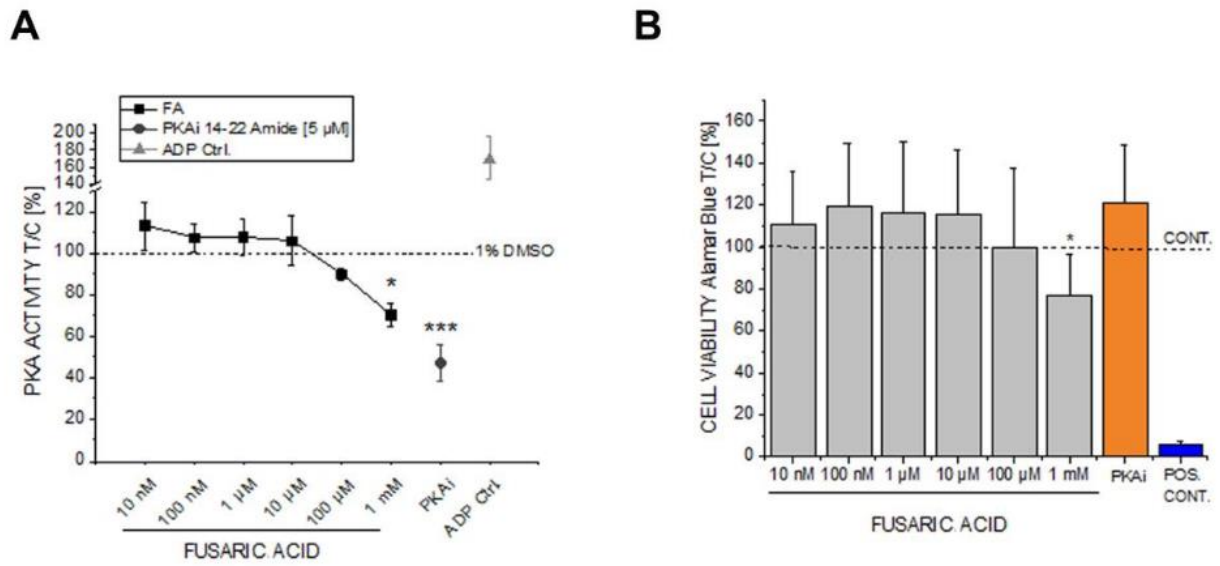

Figure 4. Cell-free inhibitory assay and cell viability results. **A.** PKA activity after 15 min of incubation with different concentrations of FA. Values are expressed in relation to the solvent control (1% DMSO) as means ± SD of in total 6 measurements acquired in 3 independent experiments (each carried out in duplicate). **B.** Cell viability measured in HCEC-1CT. Data are mean of n > 3 independent experiments ± SD. Significant differences were assessed by one-way ANOVA, followed by Fisher LSD post-hoc testing, and are indicated by "*" ($p<0.05$), "**" ($p<0.01$) and "***" ($p<0.001$). The significance was further confirmed with Bonferroni, Scheffe, Tukey, Sidak, Fisher, Bonholm and Sidakholm post hoc tests ($p < 0.05$).

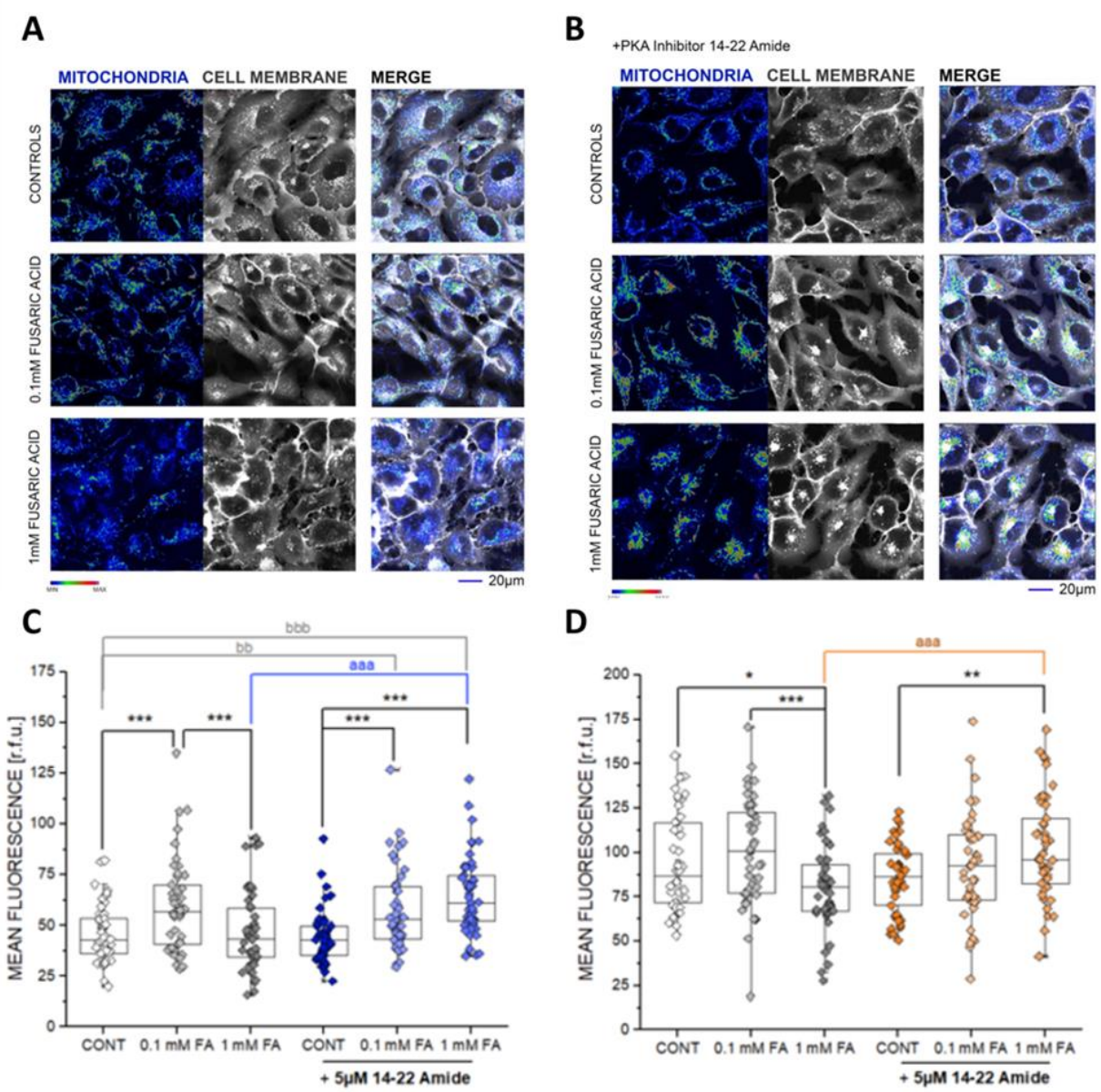

Figure 5. Results of live cell imaging. **A**. Appearance of the mitochondrial network in HCEC-1CT cells in control conditions and after 24h incubation with FA. Mean fluorescence intensity is represented in pseudocolors blue (min) red-purple (max), in grey appearance of the cell membrane. **B**. Appearance of the mitochondrial network in HCEC-1CT cells in control conditions and after 24h incubation with FA in presence of the PKA inhibitor 14-22 amide (5µM). Mean fluorescence intensity is represented in pseudocolors blue (min) red-purple (max), in grey appearance of the cell membrane. **C**. Quantification of the mean fluorescence intensity of the mitochondrial network in HCEC-1CT cells in control conditions (white diamonds) and after 24h incubation with FA (grey diamonds) and in presence of the PKA inhibitor 14-22 amide (5µM, blue diamonds). **D.** Mean fluorescence intensity of the cell membrane in HCEC-1CT cells in control conditions (white diamonds) and after 24h incubation with FA (grey diamonds) and in presence of the PKA inhibitor 14-22 amide (5µM, orange diamonds). Data result from the quantification of n = 45 cells. * indicates significant difference within the treatment groups (One way ANOVA followed

622 by Fisher LSD post-hoc testing * $p < 0,05$, ** $p < 0,01$ and *** $p < 0,001$). Letter “a”indicates significant
623 difference in comparison to the same treatment without 14-22 amide (aaap < 0.001) and “b” indicates
624 significant difference in comparison to solvent controls (bb $p < 0.01$ and bbb $p < 0.001$).

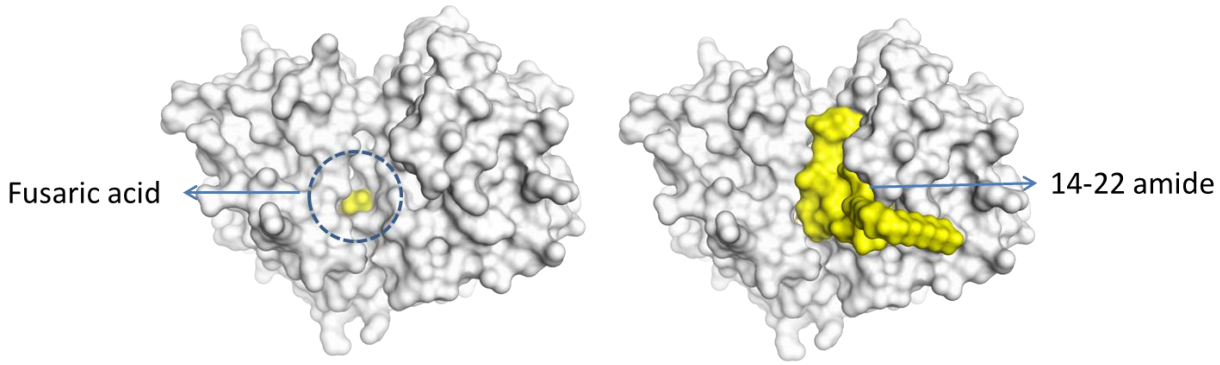

625
626 **Figure 6.** Graphical representation of PKA in complex with FA or 14-22 amide. The protein is represented
627 in white surface, while FA and 14-22 amide in yellow surface.